Desalination and Water Treatment
www.deswater.com

doi: 10.5004/dwt.2022.28566

264 (2022) 270–279
July

Preparation and characterization of a spherical Cu/Mn/Ce ternary nanocomposite oxide with high adsorption efficiency of tetracycline

Bai Sun[a,b,*], Haiyan Zhou[a], Jie Zhang[a], Angang Hu[a], Jie Mao[a], Yun Wang[a], Xiangxiang Wang[a], Shuguang Zhu[a]

[a]*Engineering Research Center of Building Energy Efficiency Control and Evaluation of the Ministry of Education, College of Environment and Energy Engineering, Anhui Jianzhu University, Hefei 230601, China, emails: bsun@mail.ustc.edu.cn (B. Sun), 1450771215@qq.com (H. Zhou), 1045441563@qq.com (J. Zhang), 1332126924@qq.com (A. Hu), 972536164@qq.com (J. Mao), 596820989@qq.com (Y. Wang), 350992818@qq.com (X. Wang), zhushuguang@ahjzu.edu.cn (S. Zhu)*
[b]*Environmental Materials and Pollution Control Laboratory, Hefei Institute of Physical Science, Chinese Academy of Sciences, Hefei 230031, China*

Received 21 November 2021; Accepted 12 May 2022

ABSTRACT

Tetracycline (TC) is a new eco toxic antibiotic, which is easy to cause bacterial drug resistance. Considering this, tetracycline in water needs to be removed. In this paper, a Cu/Mn/Ce oxide composite were prepared by a simple coprecipitation method and used as a new and efficient adsorbent to remove tetracycline from water. The morphology and microstructure of the adsorbent were characterized by scanning electron microscopy, energy-dispersive X-ray spectroscopy, Fourier-transform infrared spectroscopy, X-ray photoelectron spectroscopy, Brunauer–Emmett–Teller, X-ray diffraction and zeta potential. The effects of adsorption isotherm, kinetics, molar ratio, initial concentration and pH value of TC solution were studied. The results show that the adsorption capacity towards TC solution is the highest when the molar ratio of Cu/Mn/Ce is 1:1:3, according to the Langmuir isotherm model. The maximum adsorption capacity is 344.83 mg/g. The maximum removal rate is 99.97% at pH = 7, and the adsorption kinetics conforms to the quasi-second-order model. The adsorption capacity of Cu/Mn/Ce is basically unchanged after three cycles, and the removal rate is still as high as 91%.

Keywords: Cu/Mn/Ce; Adsorption; Nanocomposite oxide; Tetracycline

1. Introduction

In recent years, with the continuous progress of science and technology and the development of industry, more and more pollutants are involved. It is found that the pollution of antibiotics is gradually increasing in the detection of water pollutants in recent years. Although the use of antibiotics in medicine has saved many lives, long-term use will lead to certain drug resistance [1,2]. Tetracycline antibiotics are often used as veterinary drugs or animal food additives. They are the most commonly used antibiotics at present. However, due to the universal application of antibiotics, they have had a series of effects on the living environment of human beings [3]. Because tetracycline antibiotics do some harm to human body, it is necessary to study the methods to remove tetracycline antibiotics from polluted water [4]. The most commonly used strategies are physical and chemical methods. In recent years, it is found that the methods used to remove antibiotics mainly include the following: photocatalytic degradation [5,6], oxidative degradation [7], electrochemical oxidative degradation [8], membrane separation technology [9], and

* Corresponding author.

adsorption degradation [10]. Among them, adsorption degradation has attracted broad attention because of its low cost, environmental friendliness, simple and convenient operation process and wide range of raw materials of adsorbent [11]. Some adsorbents have been developed and used to remove antibiotics in the field include metal organic framework [12,13], activated carbon [14,15], natural clay minerals [16,17], engineering nanomaterials [18], etc. However, these materials are not suitable for large-scale water treatment. From the perspective of economy and practicality, we need to study an adsorbent with low cost, simple and easy production method and high efficiency for adsorption and degradation [19,20]. Although precious metals have high activity, they are expensive and vulnerable to the influence of intermediate products, which will reduce the efficiency of adsorbents. Therefore, such metals are generally not selected. Therefore, we must consider whether they are economical and feasible when selecting adsorbent raw materials [21]. A series of results show that the catalysts loaded with transition metal oxides such as copper, manganese and cerium have good reusability [22,23]. Copper is very common in daily life, and the price is cheaper than other metal elements. At the same time, cerium is also a good raw material for catalyst [24]. There are many manganese elements in natural water [25]. Therefore, it is a good choice to synthesize these three elements to prepare an economical and efficient adsorbent for removing tetracycline antibiotics in water.

In this paper, a simple coprecipitation method was used to prepare Cu/Mn/Ce oxide as an adsorbent. The adsorption kinetics and adsorption isotherm of the adsorbent were studied. The adsorbent was characterized by scanning electron microscope, X-ray diffraction, Fourier-transform infrared spectroscopy, zeta potential and energy spectrum analysis. In addition, through batch test, the influence of pH on the adsorption performance was studied, the optimal pH value was determined, and the influence of adsorbent dosage on the whole experiment was studied when the concentration and volume of tetracycline solution were determined.

2. Experimental

2.1. Reagents and instruments

The main reagents used in the experiment are directly used without further purification. The chemicals contain copper nitrate trihydrate ($Cu(NO_3)_2{\cdot}3H_2O$), ceria solid (CeO_2), manganese acetate tetrahydrate $Mn(CH_3COO)_2{\cdot}4H_2O$, anhydrous ethanol, which were analytically pure from Xilong Scientific Co., Ltd., (China). Deionized water was prepared by FST-TOP-A24 super pure water equipment by Shanghai Fushite Instrument Equipment Co., Ltd., (China).

The X-ray diffraction (XRD) patterns of the adsorbents were performed on a D/Max IIIA X-ray Diffractometer (Rigaku Co., Japan), using Cu Kα ($\lambda_{K\alpha1}$ = 1.5418 Å) as the radiation source in the range of 5°–80°. Scanning electron microscopy (SEM) was performed on Zeiss Auriga microscope. The energy-dispersive X-ray spectrum (EDS) was performed on a Zeiss Auriga microscope equipped with an Oxford Inca X-Max 50 detector. The Fourier-transform infrared spectroscopy (FTIR) of the adsorbents before and after adsorption were recorded with a Nexus 870 FTIR spectrometer in the range of 4,000–400 cm^{-1}. The X-ray photoelectron spectra (XPS) were recorded on a Thermo ESCALAB250Xi spectrometer with an excitation source of monochromatized Al Ka (hν = 1,486.6 eV) and a pass energy of 30 eV. The Brunauer–Emmett–Teller (BET) surface area was also measured. The wavelength change of the adsorbent was recorded in the range of 190–900 cm^{-1} using a UV-2600i UV-Vis spectrophotometer, Shimadzu (China) Co., Ltd.

2.2. Preparation of adsorbent

Cu/Mn/Ce oxide (CMC) composite with a molar ratio of 1:1:3 was prepared by a coprecipitation method. The preparation method is described as follows, Cu $(NO_3)_2{\cdot}3H_2O$, Mn $(CH_3COO)_2{\cdot}4H_2O$ and CeO_2 solids with Cu/Mn/Ce molar ratio of 1:1:3 were dissolved in distilled water, and the pH value was adjusted to 9.0 with Na_2CO_3 solution. The solution was aged for 4 h. The precipitate was washed several times with deionized water, and the precipitate was dried and calcined to obtain the final experimental material. Meanwhile, CMC with molar ratios of 1:1:1 and 1:1:2 were prepared according to the above methods.

2.3. Batch adsorption experiments

The tetracycline antibiotics were used as antibiotics in our study. Tetracycline was simulated with different concentrations of tetracycline solution. Three materials with different molar ratios were added with 15 mg adsorbent into 100 mL and 20 mg/L tetracycline (TC) solution for batch adsorption research. The whole experiment was conducted in a constant temperature oscillation box with shading, and the rotating speed was 160 rpm. After waiting for adsorption equilibrium, a certain amount of supernatant was taken to measure the absorbance value at the absorption wavelength of 357 nm with UV-Vis. The effects of adsorbent dosage and initial pH of TC solution on the experiment were studied by the same experimental method, and its kinetics and isotherm were studied and the results were analyzed.

The adsorption capacity and removal rate were calculated by Eqs. (1) and (2), respectively.

$$q_e = \frac{\left(C_0 - C_e\right)\cdot V}{m} \tag{1}$$

$$\eta = \frac{\left(C_0 - C_e\right)}{C_0} \times 100\% \tag{2}$$

where C_0 and C_e represent the initial and equilibrium tetracycline concentrations (mg/L), V (mL) represents the volume of the solution, and m (g) represents the amount of adsorbent.

2.4. Adsorption kinetics

In order to further analyze the adsorption kinetics, linear and nonlinear adsorption kinetic models are used to

describe the experimental data. The use of nonlinear models is to reduce the error caused by the conversion of nonlinear models to linear models [26–28].

The linear equations of the two dynamic models are as follows:

$$\log\left(q_e - q_t\right) = \log q_e - \frac{k_1 t}{2.303} \tag{3}$$

$$\frac{t}{q_t} = \frac{1}{k_2 q_e^2} + \frac{1}{q_e} \tag{4}$$

where q_e and q_t (mg/g) are the amount of TC adsorbed at equilibrium and at any time, respectively; t (min) is the adsorption time; k_1 (min^{-1}) and k_2 (g/(mg min)) are the rate constants of pseudo-first-order reaction and pseudo-second-order reaction respectively, the corresponding adsorption kinetics parameters are listed in Table 1.

In order to better understand the adsorption behavior of TC on adsorbent, the effect of contact time on TC adsorption by CMC was studied. As shown in Fig. 1a, with the extension of the contact time in the initial stage, the adsorption capacity increases significantly, and then increases slowly. The adsorption was in the equilibrium stage after 540 min, and reached the maximum adsorption capacity within 720 min. The rapid adsorption of TC at the beginning of the reaction is attributed to the existence of a large number of unoccupied adsorption sites on the adsorbent surface, which enables TC to interact rapidly [29]. When the active functional sites are gradually occupied, the adsorption process becomes slow and reaches equilibrium. It can be seen from Fig. 1b, c and Table 1 that compared with the pseudo-first-order kinetic model, the pseudo-second-order kinetic model (R^2 = 0.993) better fits the kinetic characteristics of TC, and it can be judged that the adsorption process of CMC on TC is mainly dominated by chemical adsorption. According to the calculation results of the pseudo-second-order kinetic model, the maximum adsorption capacity of CMC for TC is 136.054 mg/g, which is very close to the experimental value of 132.894 mg/g when the initial TC concentration is 20 mg/L. Adsorption time of 720 min was selected for further experiments to ensure adsorption equilibrium.

2.5. Adsorption isotherm

Freundlich and Langmuir models were used to verify the accurate mechanism of the adsorption process and calculate the adsorption capacity [30–32]. In order to study the adsorption properties, Freundlich and Langmuir models and linear equations were used.

The two linear model equations are as follows:

$$\frac{C_e}{q_e} = \frac{C_e}{q_{\max}} + \frac{1}{K_L \cdot q_{\max}} \tag{5}$$

$$\ln q_e = \frac{1}{n}\ln C_e + \ln K_F \tag{6}$$

where C_e (mg/L) is the TC concentration after equilibrium adsorption; q_e (mg/g) is the amount of TC removed per weight of adsorbent after equilibrium; $q_{\max}$ (mg/g) is the maximum adsorption capacity calculated according to Langmuir equation; K_L (L/mg) is Langmuir adsorption constant; K_F (mg/g) is Freundlich adsorption constant; 1/n is a heterogeneous factor.

Table 1
Pseudo-first-order and pseudo-second-order kinetic parameters of TC adsorption by CMC

Dynamic model pseudo-first-order dynamics			Quasi-second-order dynamics		
k_1 (min^{-1})	q_e (mg/g)	R^2	k_2 (g/(mg min))	q_e (mg/g)	R^2
0.003	100.756	0.991	0.229×10^{-3}	136.054	0.993

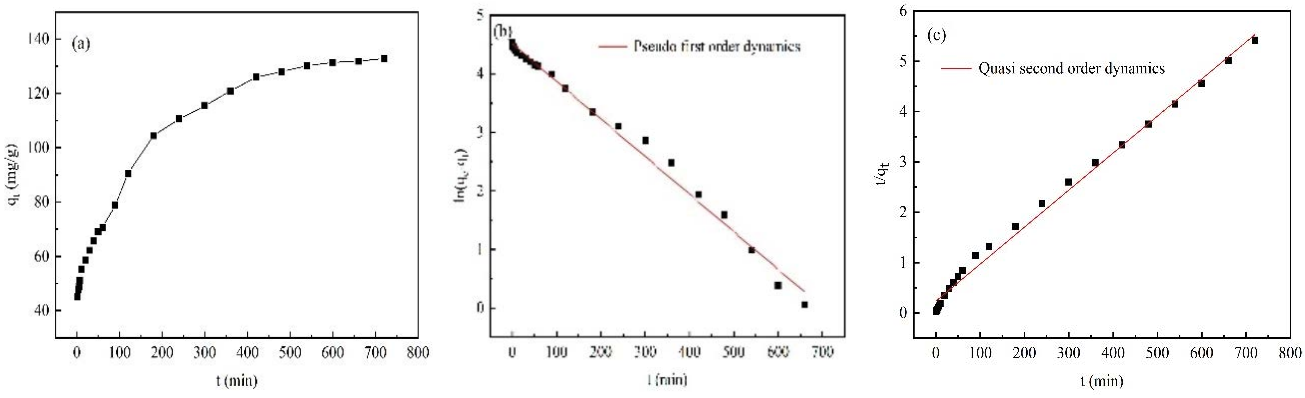

Fig. 1. (a) Kinetic data of TC adsorption by CMC, (b) pseudo-first-order kinetic curve, and (c) pseudo-second-order kinetic curve.

Fig. 2 shows the fitting of Langmuir and Freundlich isotherm models to experimental data [33,34], and the corresponding isotherm model parameters are listed in Table 2. It can be seen that Langmuir model can better fit the experimental data because of its high coefficient (R^2 = 0.996). In addition, the maximum adsorption capacity fitted by Langmuir model is 344.83 mg/g, which is almost consistent with the 344.27 mg/g measured when the initial TC concentration is 100 mg/L. The results show that the adsorption towards TC can be described by Langmuir isotherm model, indicating that the adsorption of CMC adsorbent to TC belongs to uniform monolayer adsorption [35]. The experimental results show that the CMC adsorbent has a good adsorption performance for TC. In addition, the comparison on the adsorption capacity with some other adsorbents is shown in Table 3.

3. Results and discussions

3.1. Sample characterization

SEM images contain information about the surface morphology, and the particle size and high pore structure of the samples [41]. Therefore, the surface morphology of the synthetic materials was characterized by SEM. As shown in Fig. 3a, the prepared adsorbent is spherical particles, the surface of the sphere is not smooth, and a large number of irregular nanoparticles gather on it. It can be speculated that these nanoparticles may be the basic unit to form a spherical structure, and some spheres form "gourd" aggregates through fusion. Fig. 3b shows the morphology and structure of the adsorbent after adsorption. TC is adsorbed in the gap and surface of the adsorbent particles, indicating that the adsorbent material has good adsorption effect.

Fig. 3c shows the elemental dispersive spectrum of CMC. The energy dispersive analysis shows that there are some manganese, copper and cerium in the composite. The largest proportion belongs to oxygen, indicating that there are a large number of oxygen-containing functional groups in the composites.

BET analysis was used to determine the physicochemical properties of CMC, including specific surface area, pore diameter and pore volume. Fig. 4a shows the adsorption and desorption isotherm s of CMC, the specific surface area of CMC is 24.1980 m^2/g, and the adsorption isotherm belongs to type III. The amount of adsorbed gas increases with the increase of component pressure. When the relative pressure reaches 1, the adsorption capacity is far from saturated, indicating that there are pores in the adsorbent. According to the BET results, the pore volume is 0.1317 cm^3/g. The average pore diameter is 21.8691 nm, indicating that the CMC is mesoporous.

The phase composition and crystal structure of Cu/Mn/Ce adsorbents prepared with different molar ratios were determined by XRD analysis. The obtained spectra are shown in Fig. 5a. The main diffraction peaks at 28.55°, 33.08°, 47.49°, 56.34°, 59.09°, 69.42°, 76.71°, 79.08°, 88.43°, correspond to (111), (200), (220), (311), (222), (400), (331), (420) and (422) planes, respectively. The diffraction peaks in the XRD patterns of adsorbents with different Cu/Mn/Ce molar ratios are basically the same. When the molar ratio of Cu/Mn/Ce is 1:1:1, there are weak double diffraction peaks at 2θ = 35.50° and 38.73°. It indicates the existence of CuO (JCPDS, No. 80-1916). When the molar ratio of adsorbent

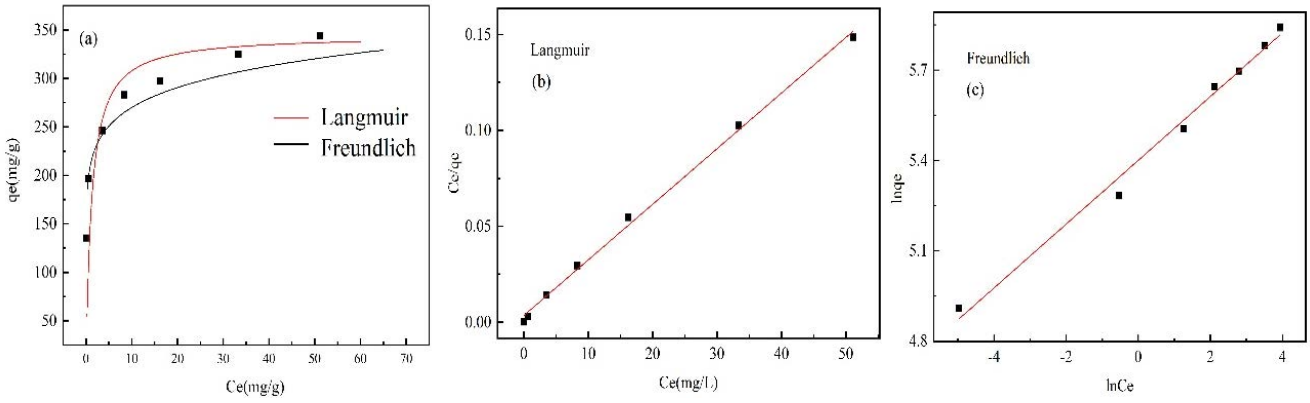

Fig. 2. (a) Isotherms of TC adsorbed by CMC, (b) and (c) linear fitting curves of Langmuir model and Freundlich model of TC adsorbed by CMC, respectively.

Table 2
Isotherm model parameters of TC adsorbed by CMC

Isotherm model		Langmuir $\left(\frac{C_e}{q_e}=\frac{C_e}{q_{max}}+\frac{1}{K_L\times q_{max}}\right)$			Freundlich $\left(\ln q_e=\frac{1}{n}\ln C_e+\ln K_F\right)$		
Parameters	K_L (L/mg)	q_{max} (mg/g)	R^2	R_L	n	K_F	R^2
Value	0.831	344.828	0.996	0.057	9.433	211.511	0.987

Table 3
Comparison of adsorption capacity of different adsorbents

Adsorbents	Temperature (°C)	pH	q_{max} (mg/g)	Reference
Clay-biochar composites	–	7–8	26	[36]
Magnetic biochar	25	3–11	42.31	[37]
MIL-88A grown *in-situ* on graphitic carbon nitride (g-C_3N_4)	–	7	154.51	[38]
Mn(II)-coated mesoporous silica nanoparticles	25	–	229	[39]
Organic framework derived porous carbon	25	–	285	[40]
CMC nanoparticles	25	7	344.83	Present work

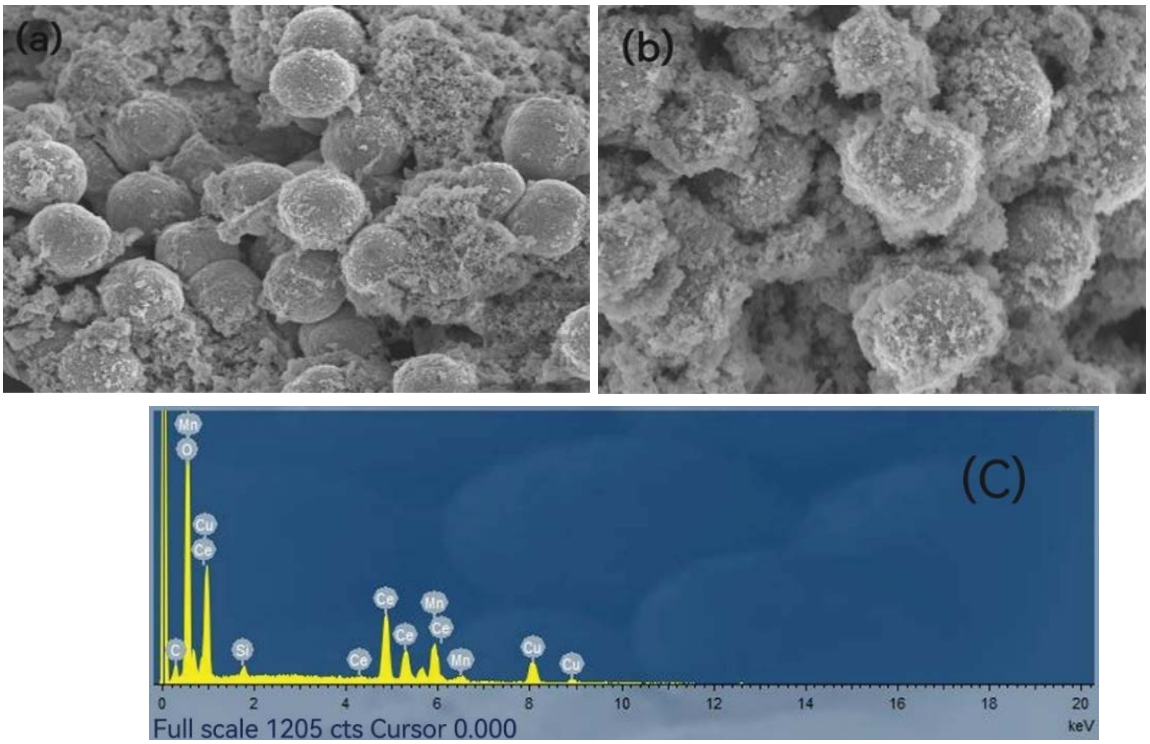

Fig. 3. (a) SEM image of before adsorption CMC nanoparticles, (b) SEM image of after adsorption CMC nanoparticles, and (c) EDS image of adsorbent with CMC.

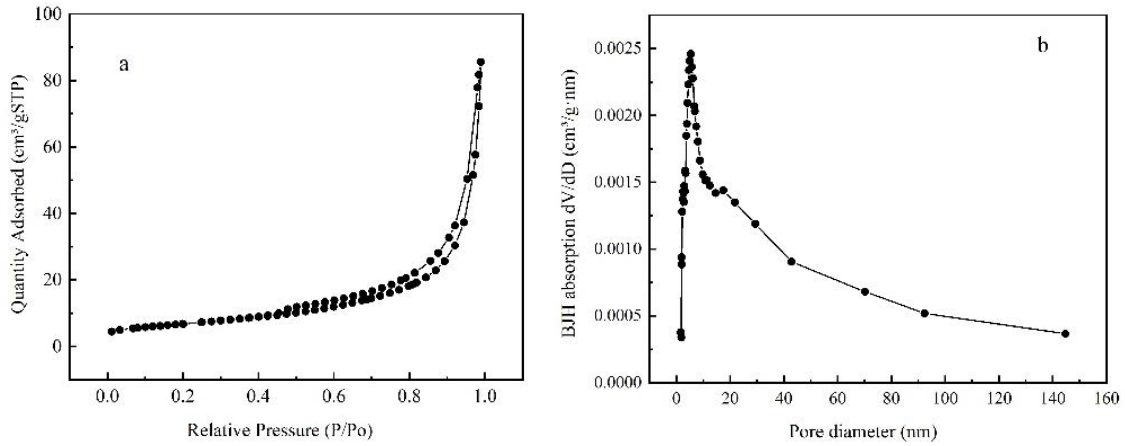

Fig. 4. BET image of CMC, (a) adsorption analysis isotherm and (b) adsorption pore volume.

Cu/Mn/Ce is 1:1:3, only clear CeO_2 structure diffraction peaks can be seen in the XRD spectrum, and no diffraction peaks related to metal copper, manganese and their oxides can be found, indicating that copper and manganese elements enter the ceria lattice to form a solid solution or exist on the surface of the adsorbent in a highly dispersed form.

The zeta potential of the adsorbent was measured, as shown in Fig. 5b. It is found that the zero potential (pH_{pzc}), that is, the pH at which the surface charge of the material becomes zero is 7.58. At this point, the number of positively charged sites is equal to the number of negatively charged sites. The surface of the material is positively charged below pH_{pzc} and can better interact with TC solution under acidic and neutral conditions.

3.2. Adsorptive property

3.2.1. Effect of molar ratio

The experimental results of the effect of adsorbent ratio on adsorption performance are shown in Fig. 6a. The adsorbent prepared under the condition of Cu/Mn/Ce molar ratio of 1:1:3 has better adsorption capacity than other ratios. This is ascribed to the main form in the composite oxide becomes CeO_2 due to the increase of Ce content, which makes Mn and Cu highly dispersed, forming more amorphous active centers to improve the adsorption capacity [42]. After continuously increasing the ratio of cerium content to more than 1:1:3, it was found that the adsorption capacity decreased during the experiment, then more cerium accumulated to form larger particles in the precipitation process.

3.2.2. Effect of adsorbent dosage

In order to determine the optimal dosage of adsorbent, the effect of CMC dosage on TC removal was studied. As can be seen from Fig. 6b, when the initial TC concentration is 20 mg/L and the solution volume is 100 mL, with the increase of adsorption dose from 5 mg to 30 mg, the adsorption capacity decreases from 256.38 to 67.76 mg/g. It may be due to the fast exposure and saturation of TC adsorption sites at low doses of CMC. However, the unit effective collision and TC concentration gradient decreased at higher CMC dose, resulting in lower TC adsorption. On the other hand, depending on the increase of adsorption dose, the removal rate of TC gradually increases. When the dosage of CMC reaches 15 mg, the adsorption reaches saturation and TC is almost removed. Therefore, the optimal adsorption dose for removing TC from aqueous

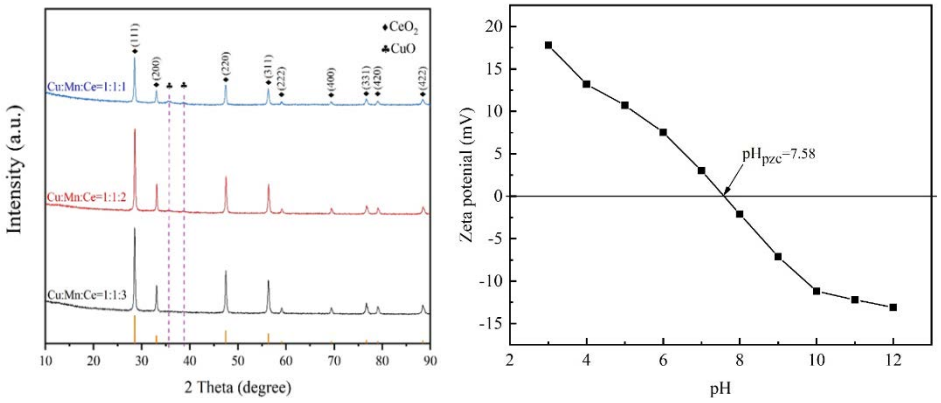

Fig. 5. (a) XRD patterns of adsorbents with different molar ratios and (b) zeta potential of CMC adsorbent.

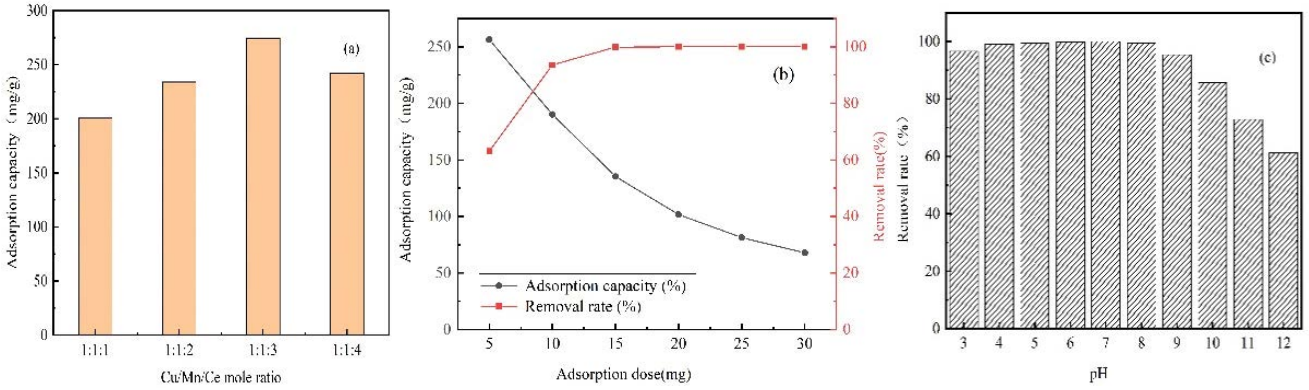

Fig. 6. (a) Effect of adsorbents with different Cu/Mn/Ce molar ratio on TC adsorption performance, (b) effect of CMC dosage on TC removal efficiency and adsorption capacity, and (c) effect of pH on TC removal by CMC adsorbent.

solution is 15 mg. Further increasing the amount of adsorbent will reduce the utilization efficiency of adsorbent.

3.2.3. Effect of pH value of solution

The pH value of solution is an important parameter affecting the surface charge of adsorbent and the morphology of TC molecule. TC molecule has three water dissociation constants (PK) according to pH value α = 3.3, 7.68 and 9.69), which exist in the form of cation (TC^+), zwitterion (TC^0) and anion (TC^-, TC^{2-}) respectively under the conditions of strong acid with pH < 3.3, medium acid to neutral with pH < 7.68 and alkaline with pH > 7.68 [43]. The effect of pH value on TC removal efficiency is shown in Fig. 6c. When the pH value of TC solution increases from 3 to 12, the removal rate of TC increases initially and then decreases subsequently, and reaches the maximal rate of 99.97% when the pH value is 7. At a low pH, the removal efficiency of adsorbent decreases slightly, which is due to the electrostatic repulsion caused by the positive charge of TC. When 4 < pH < 8, TC molecules mainly exist in the form of zwitterions. They are almost neutral and are unilaterally electrostatic attracted by positively charged metal complexes. When pH > 8, the pH_{pzc} = 7.58 of the adsorbent is less than the pH value, and the surface of the adsorbent is negatively charged. Therefore, electrostatic repulsion occurs between negatively charged CMC and anionic TC, resulting in the reduction of TC removal rate. Under the condition of strong acidity and alkalinity of the solution, most TC is still removed, which indicates that in addition to electrostatic action, there are other functions, such as π–π conjugation and hydrogen bond, which participate in the adsorption process [44]. In short, it seems undesirable to carry out the experiment under low or high pH conditions, so the follow-up experiment is carried out at pH = 7.

3.3. Adsorption mechanism

The functional groups and atomic and molecular vibrations were identified by FTIR spectroscopy. The structure of CMC nanoparticles before and after adsorption was analyzed by FTIR spectroscopy, as shown in Fig. 7. When the infrared spectrum band is at 1,350 cm^{-1}, the absorption peak becomes more sharp due to the stretching vibration of benzene ring in tetracycline. The strong absorption peak at 3,420 cm^{-1} is due to –OH vibration [45], and the sharp absorption peak at 1,380 cm^{-1} is due to $–CH_3$ bending [46]. The absorption peak at 1,600 cm^{-1} is caused by the stretching vibration of C=C or the symmetrical and asymmetric vibration of C=O [47], while the shift of the absorption peak at 529 cm^{-1} is related to the vibration of Ce–O. It can be seen from XRD analysis that pure CeO_2 phase is formed [48–50]. The absorption peaks at 2,810 and 1,120 cm^{-1} are prominent due to the symmetrical and asymmetric stretching of C–H and the vibration stretching of C–O [51], and the absorption peak at 766 cm^{-1} is caused by the stretching vibration of Mn–OH [52].

The composition on the surface of CMC before and after adsorption was analyzed by XPS. In Fig. 8, the C 1s spectra before and after adsorption are fitted into three separate peaks at 284.82, 286.76 and 289.64 eV, which correspond to the binding energy of C–C/C–H, C–O–C and C=O. It can be seen from that C–O–C increases from 0 before adsorption to 32.48%. The O 1s spectra before and after adsorption are fitted into four separate peaks at 532.24, 529.47, 531.06 and 531.82 eV, corresponding to ceria, Cu–O, CeO_2, C=O and –OH respectively. It can be seen that the proportions of C=O and –OH increase from 0 to 11.56% and 22.41% respectively, which verify that CMC adsorbs a large amount of tetracycline [53–55].

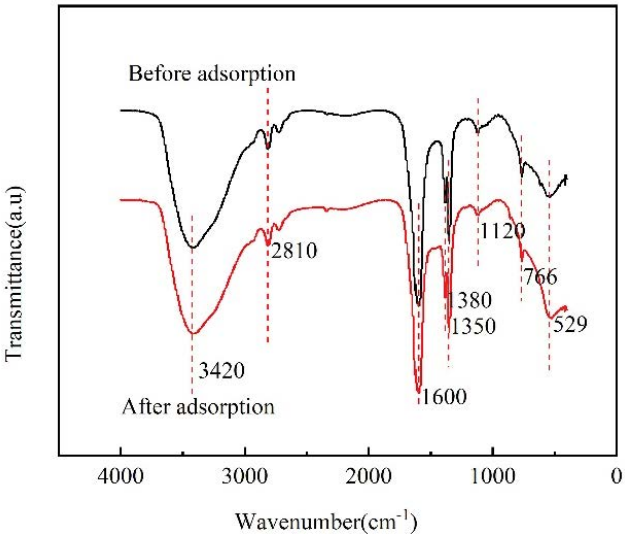

Fig. 7. Infrared spectra before and after CMC adsorption.

3.4. Cyclic regeneration experiment

The regeneration and repeatability of adsorbent are very important for practical application. The recycling experiment of CMC was further studied, 100 mL of TC solution with an initial concentration of 20 mg/L was taken into a conical flask, then, 15 mg of saturated adsorbent was added. Finally, the regeneration experiment was conducted four times according to the above steps. Fig. 9 shows the effect of adsorbent regeneration times on TC adsorption capacity. After continuous use for three times, the adsorption capacity of TC did not change significantly. After the fifth cycle, the removal rate of TC remained above 91%. The results show that CMC not only has high TC adsorption capacity, but also has high repeatability.

4. Conclusion

CMC adsorbent was synthesized by a simple coprecipitation method. When the molar ratio of Cu/Mn/Ce was 1:1:3, the samples exhibited a high adsorption capacity for TC. Through the analysis of Langmuir and Freundlich isotherm models, the Langmuir isotherm model is better than Freundlich isotherm model in fitting the experimental results. According to the Langmuir isotherm model, the maximum adsorption capacity is 344.83 mg/g, and the maximum removal rate of the material at pH = 7 is as high as 99.97%. The high removal rate provides a good basis for the study of tetracycline removal from wastewater.

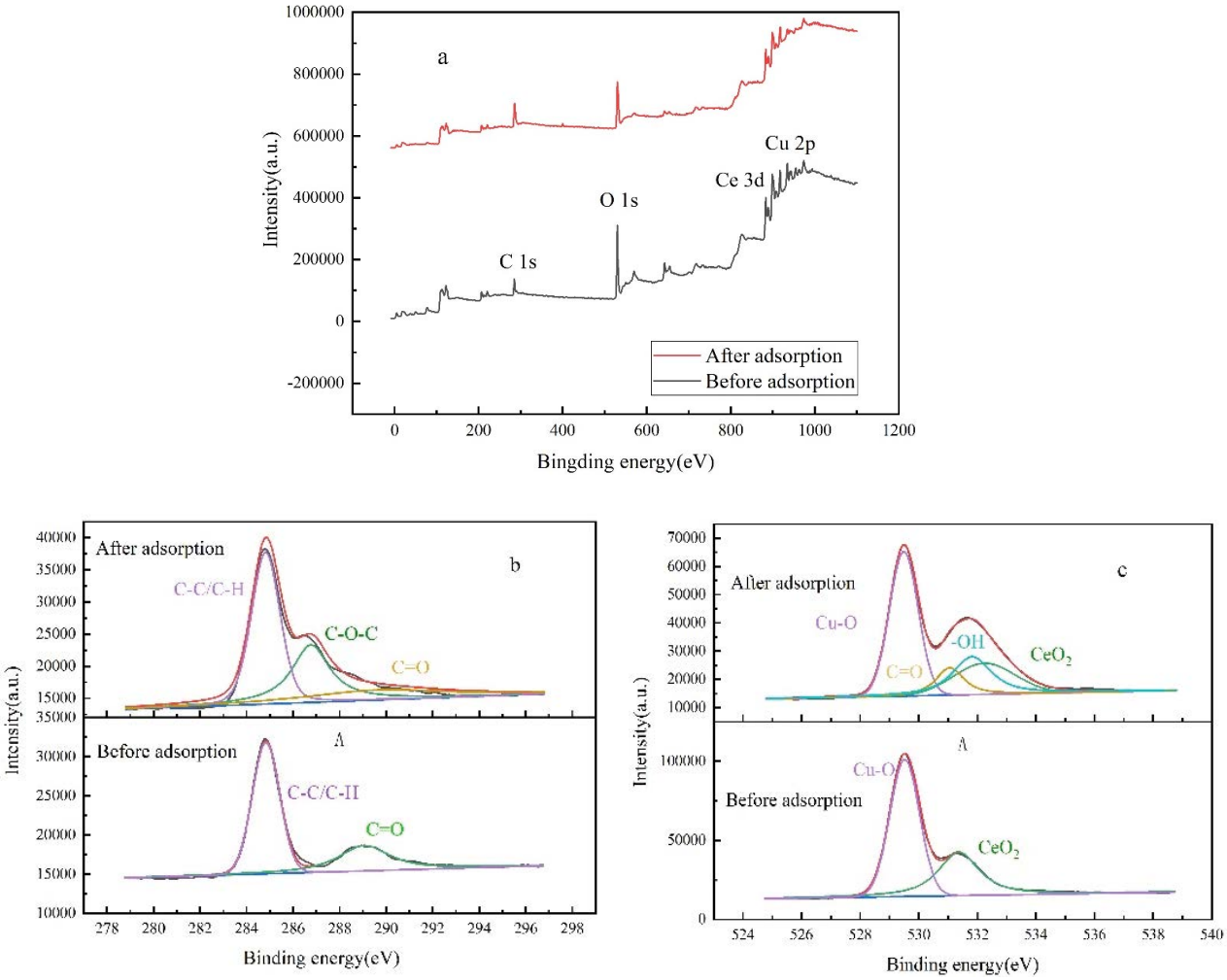

Fig. 8. (a) X-ray photoelectron spectroscopy before and after CMC adsorption, (b) C 1s spectrum before and after adsorption, and (c) O 1s spectrum before and after adsorption.

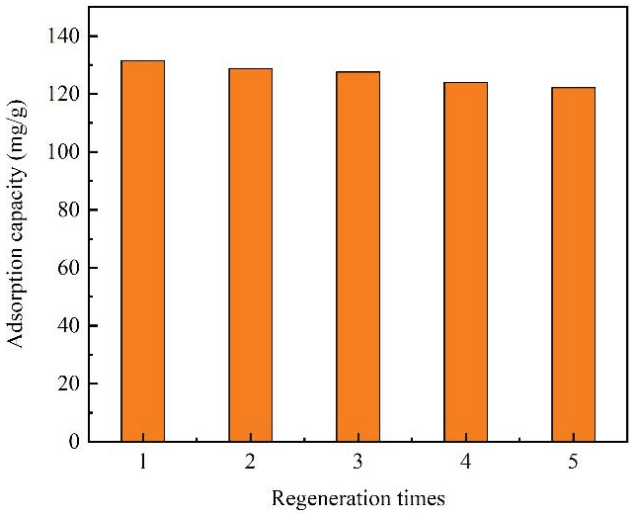

Fig. 9. Cyclic regeneration diagram of TC solution adsorbed by CMC.

Acknowledgments

The authors are especially grateful to the Project of National Key Research and Development Program (2019YFC0408503), the Natural Science Research Project of the Higher Education Institutions of Anhui Province (KJ2021A0616, KJ2020A0468), the National Natural Science Foundation of China (52103104, 61873003), the Natural Science Foundation of Anhui Province (1908085QE241), the first batch of natural science projects supported by surplus funds in 2021 of Anhui Jianzhu University (JZ202129, JZ202134) and the Scientific Research Start-up Foundation for Introduction of Talent, Anhui Jianzhu University (2016QD113).

References

[1] Y.R. Gu, S.Z. Shen, B.J. Han, X.L. Tian, F.X. Yang, K.Q. Zhang, Family livestock waste: an ignored pollutant resource of antibiotic resistance genes, Ecotoxicol. Environ. Saf., 197 (2020) 110567, doi: 10.1016/j.ecoenv.2020.110567.

[2] L.J. Niu, G.M. Zhang, G. Xian, Z.J. Ren, T. Wei, Q.G. Li, Y. Zhang, Z.G Zou, Tetracycline degradation by persulfate activated

with magnetic γ-Fe_2O_3/CeO_2 catalyst: performance, activation mechanism and degradation pathway, Sep. Purif. Technol., 259 (2021) 118156, doi: 10.1016/j.seppur.2020.118156.
[3] M. Wu, C. Wang, Y. Zhao, L. Xiao, C. Zhang, X. Yu, B. Luo, B.O. Hu, W. Fan, W. Shi, Hydrothermal synthesis of porous rh-In_2O_3 nanostructures with visible-light-driven photocatalytic degradation of tetracycline, Cryst. Eng. Comm., 17 (2015) 2336–2345.
[4] Y. Yue, Y.-J. Liu, J.C. Wang, R. Vukanti, Y. Ge, Enrichment of potential degrading bacteria accelerates removal of tetracyclines and their epimers from cow manure biochar amended soil, Chemosphere, 278 (2021) 130358, doi: 10.1016/j.chemosphere.2021.130358.
[5] Y.P. Li, X.L. Sun, Y.M. Tang, Y.H. Ng, L.T.Li, F. Jiang, J. Wang, W.R. Chen, L.S. Li, Understanding photoelectrocatalytic degradation of tetracycline over three-dimensional coral-like ZnO/$BiVO_4$ nanocomposite, Mater. Chem. Phys., 271 (2021) 124871, doi: 10.1016/j.matchemphys.2021.124871.
[6] Q.Q. Xu, H. Yi, C. Lai, G.M. Zeng, D.L. Huang, M.F. Li, Z.W. An, X.Q. Huo, L. Qin, S.Y. Liu, B.S. Li, M.M. Zhang, X.G. Liu, L. Chen, Construction of 2D/2D nano-structured rGO-BWO photocatalysts for efficient tetracycline degradation, Catal. Commun., 124 (2019) 113–117.
[7] W.L. Shi, F. Guo, H.B. Wang, M.M. Han, H. Li, S.L. Yuan, H. Huang, Y. Liu, Z.H. Kang, Carbon dots decorated the exposing high-reactive (111) facets CoO octahedrons with enhanced photocatalytic activity and stability for tetracycline degradation under visible light irradiation, Appl. Catal., B, 219 (2017) 36–44.
[8] S.F. Tang, M.Z. Zhao, D.L. Yuan, X. Li, X.Y. Zhang, Z.B. Wang, T.F. Jiao, K. Wang, $MnFe_2O_4$ nanoparticles promoted electrochemical oxidation coupling with persulfate activation for tetracycline degradation, Sep. Purif. Technol., 255 (2021) 117690, doi: 10.1016/j.seppur.2020.117690.
[9] A. Giacobbo, A. Meneguzzi, A.M. Bernardes, M.N. de Pinho, Pressure-driven membrane processes for the recovery of antioxidant compounds from winery effluents, J. Cleaner Prod., 155 (2017) 172–178.
[10] A. Maged, J. Iqbal, S. Kharbish, I.S. Ismael, A. Bhatnagar, Tuning tetracycline removal from aqueous solution onto activated 2:1 layered clay mineral: characterization, sorption and mechanistic studies, J. Hazard. Mater., 384 (2020) 121320, doi: 10.1016/j.jhazmat.2019.121320.
[11] M. Karpov, B. Seiwert, V. Mordehay, T. Reemtsma, T. Polubesova, B. Chefetz, Transformation of oxytetracycline by redox-active Fe(III)- and Mn(IV)-containing minerals: processes and mechanisms, Water Res., 145 (2018) 136–145.
[12] X.L. Song, Y. Wang, T. Zhu, J.L. Liu, S.W. Zhang, Facile synthesis a novel core–shell amino functionalized MIL-125(Ti) micro-photocatalyst for enhanced degradation of tetracycline hydrochloride under visible light, Chem. Eng. J., 416 (2021) 129126, doi: 10.1016/j.cej.2021.129126.
[13] Y.H. Ma, M.Y. Li, J.J. Jiang, T.R. Li, X.Y. Wang, Y.Y. Song, S.S. Dong, In-situ prepared MIL-53(Fe)/BiOI photocatalyst for efficient degradation of tetracycline under visible-light driven photo-Fenton system: investigation of performance and mechanism, J. Alloys Compd., 870 (2021) 159524, doi: 10.1016/j.jallcom.2021.159524.
[14] Y. Gao, Q. Wang, G.Z. Ji, A.M. Li, Degradation of antibiotic pollutants by persulfate activated with various carbon materials, Chem. Eng. J., 429 (2022) 132387, doi: 10.1016/j.cej.2021.132387.
[15] Z.Q. Yang, Y. Li, X.Y. Zhang, X.D. Cui, S. He, H. Liang, A. Ding, Sludge activated carbon-based $CoFe_2O_4$-SAC nanocomposites used as heterogeneous catalysts for degrading antibiotic norfloxacin through activating peroxymonosulfate, Chem. Eng. J., 384 (2020) 123319, doi: 10.1016/j.cej.2019.123319.
[16] J. Cuevas, N. Dirocie, F. Yunta, C.G. Delgado, D.E. González Santamaría, A.I. Ruiz, R. Fernández, E. Eymar, Evaluation of the sorption potential of mineral materials using tetracycline as a model pollutant, Minerals, 9 (2019) 453, doi: 10.3390/min9070453.
[17] L. Jia, R.J. Chen, J. Xu, L.N. Zhang, X.Z. Chen, N. Bi, J. Gou, T.Q. Zhao, A stick-like intelligent multicolor nano-sensor for the detection of tetracycline: the integration of nano-clay and carbon dots, J. Hazard. Mater., 413 (2021) 125296, doi: 10.1016/j.jhazmat.2021.125296.
[18] W. Wang, J.J. Fang, H. Chen, Nano-confined g-C_3N_4 in mesoporous SiO_2 with improved quantum size effect and tunable structure for photocatalytic tetracycline antibiotic degradation, J. Alloys Compd., 819 (2020) 153064, doi: 10.1016/j.jallcom.2019.153064.
[19] Y.M. Hunge, A.A. Yadav, S.W. Kang, H. Kim, Photocatalytic degradation of tetracycline antibiotics using hydrothermally synthesized two-dimensional molybdenum disulfide/titanium dioxide composites, J. Colloid Interface Sci., 606 (2022) 454–463.
[20] D. Hao, Y.F. Chen, Y. Zhang, N. You, Nanocomposites of zero-valent iron@biochar derived from agricultural wastes for adsorptive removal of tetracyclines, Chemosphere, 284 (2021) 131342, doi: 10.1016/j.chemosphere.2021.131342.
[21] X.X. Huang, N.W. Zhu, X.R. Wei, Y. Ding, Y.X. Ke, P.X. Wu, Z.H. Liu, Mechanism insight into efficient peroxydisulfate activation by novel nano zero-valent iron anchored yCo_3O_4 (nZVI/yCo_3O_4) composites, J. Hazard. Mater., 400 (2020) 123157, doi: 10.1016/j.jhazmat.2020.123157.
[22] J. Chen, X.I. Chen, W. Xu, Z. Xu, J. Chen, H. Jia, J. Chen, Hydrolysis driving redox reaction to synthesize Mn-Fe binary oxides as highly active catalysts for the removal of toluene, Chem. Eng. J., 330 (2017) 281–293.
[23] Y.U. Wang, D. Yang, S. Li, L. Zhang, G. Zheng, L. Guo, Layered copper manganese oxide for the efficient catalytic CO and VOCs oxidation, Chem. Eng. J., 357 (2019) 258–268.
[24] C. Wang, C.H. Zhang, W.C. Hua, Y.L. Guo, G.Z. Lu, S. Gil, A. Giroir-Fendler, Catalytic oxidation of vinyl chloride emissions over Co-Ce composite oxide catalysts, Chem. Eng. J., 315 (2017) 392–402.
[25] Y.H. Bai, J.F. Su, Q. Wen, G.Q. Li, L. Xue, T.L. Huang, Removal of tetracycline by denitrifying Mn(II)-oxidizing bacterium *Pseudomonas* sp. H117 and biomaterials (BMO and MBMO): efficiency and mechanisms, Bioresour. Technol., 312 (2020) 123565, doi: 10.1016/j.biortech.2020.123565.
[26] S. Mallakpour, E. Khadem, Linear and nonlinear behavior of crosslinked chitosan/N-doped graphene quantum dot nanocomposite films in cadmium cation uptake, Sci. Total Environ., 690 (2019) 1245–1253.
[27] M. Moradi, M. Heydari, M. Darvishmotevalli, K. Karimyan, V.K. Gupta, Y. Vasseghian, H. Sharafi, Kinetic and modeling data on phenol removal by Iron-modified Scoria Powder (FSP) from aqueous solutions, Data Brief, 20 (2018) 957–968.
[28] M. Heydari, K. Karimyan, M. Darvishmotevalli, A. Karami, Y. Vasseghian, N. Azizi, M. Ghayebzadeh, M. Moradi, Data for efficiency comparison of raw pumice and manganese-modified pumice for removal phenol from aqueous environments—application of response surface methodology, Data Brief, 20 (2018) 1942–1954.
[29] Z. Zhang, Y. Chen, C.Y. Hu, C. Zuo, P. Wang, W.Q. Chen, T.Q. Ao, Efficient removal of tetracycline by a hierarchically porous ZIF-8 metal organic framework, Environ. Res., 198 (2021) 111254, doi: 10.1016/j.envres.2021.111254.
[30] S. Sahu, P. Kar, N. Bishoyi, L. Mallik, R.K. Patel, Synthesis of polypyrrole-modified layered double hydroxides for efficient removal of Cr(VI), J. Chem. Eng. Data, 64 (2019) 4357–4368.
[31] M. Moradi, O.B. Naeej, A. Azari, A.M. Bandpei, A.J. Jafari, A. Esrafili, R.R. Kalantary, A comparative study of nitrate removal from aqueous solutions using zeolite, nZVI–zeolite, nZVI and iron powder adsorbents, Desal. Water. Treat., 74 (2017) 278–288.
[32] N. Osouleddini, M. Moradi, T. Khosravi, R. Khamotian, H. Sharafi, The iron modification effect on performance of natural adsorbent scoria for malachite green dye removal from aquatic environments: modeling, optimization, isotherms, and kinetic evaluation, Desal. Water Treat., 123 (2018) 348–357.
[33] H.N. Tran, S.-J. You, A. Hosseini-Bandegharaei, H.-P. Chao, Mistakes and inconsistencies regarding adsorption of contaminants from aqueous solutions: a critical review, Water Res., 120 (2017) 88–116.

[34] E.C. Lima, A.A. Gomes, H.N. Tran, Comparison of the nonlinear and linear forms of the van't Hoff equation for calculation of adsorption thermodynamic parameters ($\Delta S°$ and $\Delta H°$), J. Mol. Liq., 311 (2020) 113315, doi: 10.1016/j.molliq.2020.113315.
[35] A. Lim, J.J. Chew, L.H. Ngu, S. Ismadji, D.S. Khaerudini, J. Sunarso, Synthesis, characterization, adsorption isotherm, and kinetic study of oil palm trunk-derived activated carbon for tannin removal from aqueous solution, ACS Omega, 5 (2020) 28673–28683.
[36] P. Borthakur, M. Aryafard, Z. Zara, R. David, B. Minofar, M.R. Das, M. Vithanage, Computational and experimental assessment of pH and specific ions on the solute solvent interactions of clay-biochar composites towards tetracycline adsorption: implications on wastewater treatment, J. Environ. Manage., 283 (2021) 111989, doi: 10.1016/j.jenvman.2021.111989.
[37] F. Gao, Z.X. Xu, Y.J. Dai, Removal of tetracycline from wastewater using magnetic biochar: a comparative study of performance based on the preparation method, Environ. Technol. Innovation, 24 (2021) 101916, doi: 10.1016/j.eti.2021.101916.
[38] S.Y. Zheng, Z. Kong, L.J. Meng, J.L. Song, N. Jiang, Y.N. Gao, J.L. Guo, T.W. Mu, M.H. Huang, MIL-88A grown in-situ on graphitic carbon nitride (g-C_3N_4) as a novel sorbent: synthesis, characterization, and high-performance of tetracycline removal and mechanism, Adv. Powder Technol., 31 (2020) 4344–4353.
[39] H. Qiao, X.X. Wang, P. Liao, C. Zhang, C.X. Liu, Enhanced sequestration of tetracycline by Mn(II) encapsulated mesoporous silica nanoparticles: synergistic sorption and mechanism, Chemosphere, 284 (2021) 131334, doi: 10.1016/j.chemosphere.2021.131334.
[40] F.-Z. Cui, R.-R. Liang, Q.-Y. Qi, G.-F. Jiang, X. Zhao, Efficient removal of Cr(VI) from aqueous solutions by a dual-pore covalent organic framework, Adv. Sustainable Syst., 3 (2019) 1800150, doi: 10.1002/adsu.201800150.
[41] N. Minju, K. Venkat Swaroop, K. Haribabu, V. Sivasubramanian, P. Senthil Kumar, Removal of fluoride from aqueous media by magnesium oxide-coated nanoparticles, Desal. Water Treat., 53 (2015) 2905–2910.
[42] U. Menon, H. Poelman, V. Bliznuk, V.V. Galvita, D. Poelman, G.B. Marin, Nature of the active sites for the total oxidation of toluene by CuO–CeO_2/Al_2O_3, J. Catal., 295 (2012) 91–103.
[43] J. Xia, Y.X. Gao, G. Yu, Tetracycline removal from aqueous solution using zirconium-based metal-organic frameworks (Zr-MOFs) with different pore size and topology: adsorption isotherm, kinetic and mechanism studies, J. Colloid Interface Sci., 590 (2021) 495–505.
[44] M. Oveisi, M.A. Asli, N.M. Mahmoodi, MIL-Ti metal-organic frameworks (MOFs) nanomaterials as superior adsorbents: synthesis and ultrasound-aided dye adsorption from multicomponent wastewater systems, J. Hazard. Mater., 347 (2018) 123–140.
[45] K.N. Wang, J.J. Wu, M.L. Zhu, Y.-Z. Zheng, X. Tao, Highly effective pH-universal removal of tetracycline hydrochloride antibiotics by UiO-66-$(COOH)_2$/GO metal–organic framework composites, J. Solid State Chem., 284 (2020) 121200, doi: 10.1016/j.jssc.2020.121200.
[46] J. Abdi, N.M. Mahmoodi, M. Vossoughi, I. Alemzadeh, Synthesis of magnetic metal-organic framework nanocomposite (ZIF-8@SiO_2@$MnFe_2O_4$) as a novel adsorbent for selective dye removal from multicomponent systems, Microporous Mesoporous Mater., 273 (2019) 177–188.
[47] J. Ma, B.Q. Zhou, H. Zhang, W.B. Zhang, Fe/S modified sludge-based biochar for tetracycline removal from water, Powder Technol., 364 (2020) 889–900.
[48] A. Umar, R. Kumar, M.S. Akhtar, G. Kumar, S.H. Kim, Growth and properties of well-crystalline cerium oxide (CeO_2) nanoflakes for environmental and sensor applications, J. Colloid Interface Sci., 454 (2015) 61–68.
[49] P.K. Sane, S. Tambat, S. Sontakke, P. Nemade, Visible light removal of reactive dyes using CeO_2 synthesized by precipitation, J. Environ. Chem. Eng., 644 (2018) 4476–4489.
[50] S. Mishra, S. Soren, A.K. Debnath, D.K. Aswal, N. Das, P. Parhi, Rapid microwave – hydrothermal synthesis of CeO_2 nanoparticles for simultaneous adsorption/photodegradation of organic dyes under visible light, Optik, 169 (2018) 125–136.
[51] X. Meng, Z.M. Liu, C. Deng, M.F. Zhu, D.Y. Wang, K. Li, Y. Deng, M.M. Jing, Microporous nano-MgO/diatomite ceramic membrane with high positive surface charge for tetracycline removal, J. Hazard. Mater., 320 (2016) 495–503.
[52] M. Minale, Z.L. Gu, A. Guadie, Y. Li, Y. Wang, Y. Meng, X.J. Wang, Hydrous manganese dioxide modified poly(sodium acrylate) hydrogel composite as a novel adsorbent for enhanced removal of tetracycline and lead from water, Chemosphere, 272 (2021) 129902, doi: 10.1016/j.chemosphere.2021.129902.
[53] S. Sicwetsha, S. Mvango, T. Nyokong, P. Mashazi, Effective ROS generation and morphological effect of copper oxide nanoparticles as catalysts, J. Nanopart. Res., 23 (2021) 227, doi: 10.1007/s11051-021-05334-x.
[54] Dr. S.C. Rood, O. Pastor-Algaba, A. Tosca-Princep, Dr. B. Pinho, Dr. M. Isaacs, Dr. L. Torrente-Murciano, Dr. S. Eslava, Synergistic effect of simultaneous doping of ceria nanorods with Cu and Cr on CO oxidation and NO reduction, Chem. Eur. J., 27 (2021) 2165–2174.
[55] R.V. Lakshmi, S.T. Aruna, S. Sampath, Ceria nanoparticles vis-à-vis cerium nitrate as corrosion inhibitors for silica-alumina hybrid sol-gel coating, Appl. Surf. Sci., 393 (2016) 397–404.